Available online at www.sciencedirect.com

ScienceDirect

Proceedings of the Combustion Institute 000 (2022) 1–10

Proceedings of the Combustion Institute

www.elsevier.com/locate/proci

Suppression of self-excited thermoacoustic instabilities by convective-acoustic interference

Eirik Æsøy[1,*], Girish K. Jankee, Srikar Yadala, Nicholas A. Worth, James R. Dawson

Department of Energy and Process Engineering, Norwegian University of Science and Technology, Trondheim N-7491, Norway

Received 5 January 2022; accepted 3 August 2022
Available online xxx

Abstract

In this paper we demonstrate direct suppression of self-excited thermoacoustic instabilities over a range of operating conditions using targeted convective-acoustic interference. Premixed hydrogen enriched methane-air flames were confined in a cylindrical pipe resulting in self-excited instabilities that corresponded to the quarter wave mode of the pipe. To suppress the instability, the phenomenon of lock-in (synchronisation) between the acoustic mode and vortex shedding from a set of cylinders placed upstream was used to produce destructive interference and suppress the self-excited modes. This was done by varying the location of the cylinders to control the convective time-delay between the convective and acoustic modes so that their combined effect on the flame response was tuned to suppress the global fluctuation of the heat release rate. This leads to a reduction in the limit-cycle amplitude and stable operation without a significant change to the flame structure. Measurements were taken over a wide range of equivalence ratios to demonstrate that the method is capable of stabilising the system for all conditions. Using a methodology which relies on time-delays related to hydrodynamic instability, rather than flame-related parameters, enables its application to fuel-flexible systems, often designed to operate within a wide range of power outputs.

Keywords: Combustion instabilities; Control; Hydrogen flames; Convective-acoustic interference

1. Introduction

Gas turbines can play a significant role in accelerating the transition to net zero carbon in power generation and aviation sectors if they burn hydrogen. In the former case, the role of the gas turbines are changing from constant base load to dynamic operation. In the latter case, the use of hydrogen fuels in aviation is more challenging. For both applications, the need to predict and prevent thermoacoustic instabilities remains a significant technical and scientific challenge [1–5].

* Corresponding author.
E-mail address: eirik.asoy@ntnu.no (E. Æsøy).
[1] text for footnote

https://doi.org/10.1016/j.proci.2022.08.033

Please cite this article as: E. Æsøy, G.K. Jankee, S. Yadala et al., Suppression of self-excited thermoacoustic instabilities by convective-acoustic interference, Proceedings of the Combustion Institute, https://doi.org/10.1016/j.proci.2022.08.033

Thermoacoustic instabilities occur when the fluctuations of heat release rate (HRR) from the combustion process couples with the fluctuations in the pressure of an acoustic mode of the combustor. Early on, it was recognised that one of the key drivers of these fluctuations was the coupling with vortex shedding (convective modes) produced by the burner geometry [6,7] which can modify the relative phase of the fluctuations (time-delay) that governs the stability of the system [8]. The time-delay, together with the gain of the flame response, depends on the geometry and operating conditions and is often characterised through the Flame Transfer Function (FTF). The FTF models the flame response as an impulse-response function that behaves as a low-pass filter where the cut-off frequency and characteristic time-delay scales with the ratio between the flame length and flow velocity [9–12]. Combined with an acoustic network model, the FTF can the be used to determine the stability of the system [13,14].

It was also recognised early on that small changes in the geometry, for example altering the position of the swirler relative to the flame, could alter the time-delay and affect stability of the system [15]. Several passive and active control strategies of combustion instabilities have exploited modifying the time-delay or phase of the system under consideration [16–18]. More recently several studies have shown that both equivalence ratio fluctuations and swirlers can directly modify the gain and phase of the FTF via convective-acoustic interactions [19–23]. These modulations were first attributed to swirl number fluctuations leading to a mode-conversion process that occurs when acoustic waves impinge on the swirler wanes [24,25]. However, similar modulations have also been observed when moving the fuel injection location leading to fluctuations in equivalence ratio [26,27].

In [11,28] modulations of the gain and phase were also observed when the swirler was replaced by cylinders which demonstrated that the underlying mechanism that modified the FTF was not only restricted to swirlers but was a more general response to convective interference. The modulations in the gain were shown to originate from the flow upstream of the flame via a hydrodynamic transfer function relating the acoustic and convective contributions to the velocity fluctuations. In this instance the convective-acoustic interference that led to modulations in the gain and phase of the FTF was due to lock-on (synchronisation) between the acoustics and the vortex shedding from the cylinders [29,30]. It was then demonstrated that the scaling of the lock-on could be used to tailor the convective-acoustic interference to modify the flame response and damp or amplify the gain of the FTF by careful placement of the cylinders [31].

The advantage of using cylinders instead of swirlers to control the level of convective-acoustic interference was threefold: (1) The natural shedding frequency follows a classical Strouhal number scaling [32], (2) the time-delay between the vortex shedding and the acoustic oscillations at the burner exit is one dimensional and therefore easily scaled [11]. In swirling flows this convective delay is more complex due to the inclusion of an azimuthal component [33]. (3) Varying the position of the cylinders upstream does not significantly change the mean flame structure compared to changes in the swirl number [22,34]. Although [31] showed that the FTF could be modified by tailoring the acoustic-convective interference by changing the upstream location of the cylinders, suppression of a self-excited instability was not demonstrated.

In this paper, we use the methodology proposed in [31] to demonstrate that it can be used to effectively control and suppress self-excited thermoacoustic instabilities in premixed flames over a wider range of operating conditions. We demonstrate that by using cylinders and following a procedure based on simple scaling parameters (described later in the paper), we are able to completely stabilise a self-excited premixed flame without any significant change to its mean structure. To the best of the authors knowledge this approach has not been explicitly demonstrated before[2], and it offers a very simple method of passive control, shown to be effective over a wide range of operating conditions, potentially well suited for fuel flexible systems.

2. Experimental setup

2.1. Geometry and operating conditions

A schematic of the burner geometry is shown in Fig. 1 and is similar to that described in previous studies [11,12,28,31]. A Cartesian coordinate system (x, y, z) is centred on the bluff body as indicated in Fig. 1(b). Premixed hydrogen enriched methane-air flames were stabilised on a bluff body with diameter 13mm mounted at the end of a rod of diameter 5 mm. Premixed air and fuel enter the base of the rig through two diametrically opposed ports before expanding into a large plenum section and then contracting into inlet pipe of diameter 19 mm. The bluff body/rod assembly is centred in the inlet pipe and is flush with the dump plane. The combustion chamber consisted of a quartz pipe of diameter 44 and height 80 mm and an extender ring equipped with a thermocouple (T_2) which enabled the length of the combustion chamber to be varied by adding steel pipes of different length

[2] A reviewer kindly pointed out that a similar effect has been observed in a ramjet combustor [35,36].

Please cite this article as: E. Æsøy, G.K. Jankee, S. Yadala et al., Suppression of self-excited thermoacoustic instabilities by convective-acoustic interference, Proceedings of the Combustion Institute, https://doi.org/10.1016/j.proci.2022.08.033

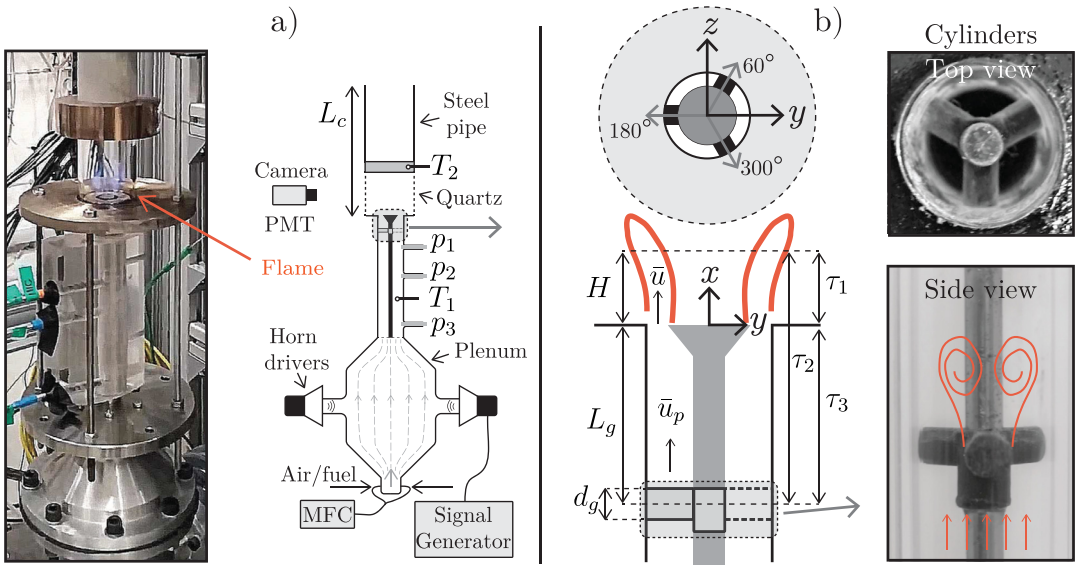

Fig. 1. Experimental setup. (a) Picture and schematic of the setup. (b) Important time, velocity and length scales and pictures of the cylinders placed upstream to generate convective/acoustic interference through synchronised vortex shedding. The top view image is taken without the bluff body to view the cylinders.

Table 1
Summary of operating conditions: N is the number of cases, L_g/d_g is the normalised distance between the cylinders to the dump plane, P_H and V_H are the hydrogen power and volume fractions, Φ the equivalence ratio, P the thermal power, and $\bar{u}$ and $\bar{u}_p$ the bulk velocities at the dump plane and in the injector pipe.

Cases	N	L_g/d_g	P_H	V_H	Φ	P [kW]	$\bar{u}$ [m/s]	$\bar{u}_p$ [m/s]
"no-cylinder"	6	32.5	0.4	0.67	0.5-0.75	2.6-3.7	10	5.7
"control-cases"	36	4–7	0.4	0.67	0.5-0.75	2.6-3.7	10	5.7

in order to find self-excited modes. The quartz pipe was long enough to visualise the whole flame.

Air and fuel were controlled using Alicat mass flow controllers (MFCs) and were premixed sufficiently far upstream to avoid equivalence ratio fluctuations. Ranges of 0–1000 and 0–50 standard litres per minute were used for the air and fuel lines, respectively. The operating conditions of the premixed hydrogen enriched methane-air flames investigated are summarized in Tab. 1. The power fraction of hydrogen was kept constant at $P_H = 0.4$ corresponding to a volume fraction $V_H = 0.67$, while the equivalence ratio Φ was varied.

2.2. Instrumentation and data acquisition

The system stability was quantified through measurements of the fluctuating components of pressure, p', and global heat release rate (HRR), Q'. The acoustic pressure p' was measured at three locations along the length of the injector pipe using Kulite XCS-093-0.35D (range 0 − 35kPa) pressure transducers (see Fig. 1(a)). The global HRR Q was measured using two Hamamatsu H11902-113 photomultiplier pipes equipped with UV band pass filters (310 ± 10 nm and 430 ± 10 nm for OH^* and CH^* chemiluminescence, respectively). The intensity is assumed to be proportional to the global HRR [37]. The signals were digitized by a 24-bit NI 9174 DAQ and sampled at a rate of 51.2 kHz.

Images of the flame were taken with a Phantom V2012 high speed camera equipped with LaVision Intensified Relay Optics (IRO) unit and a Cerco 2178 UV lens. An OH^*-filter (310 ± 10 nm) was added to capture the HRR and the images were sampled at 10 kHz in the $x - y$ plane. Additionally, the temperature was recorded using two thermocouples, one placed in the cold reactants T_1, and a second placed in the combustion chamber T_2. These were used to ensure thermal equilibrium before taking measurements of pressure and HRR.

2.3. Application of the instability control procedure

A combustion chamber length of $L_c = 430$ mm was chosen as it results in a self-excited instability at around 400 Hz which corresponds to the quarter wave mode of the pipe. The aim is to damp a given instability by moving the cylinders, see Fig. 1(b), to a location L_g where the convective-acoustic inter-

Please cite this article as: E. Æsøy, G.K. Jankee, S. Yadala et al., Suppression of self-excited thermoacoustic instabilities by convective-acoustic interference, Proceedings of the Combustion Institute, https://doi.org/10.1016/j.proci.2022.08.033

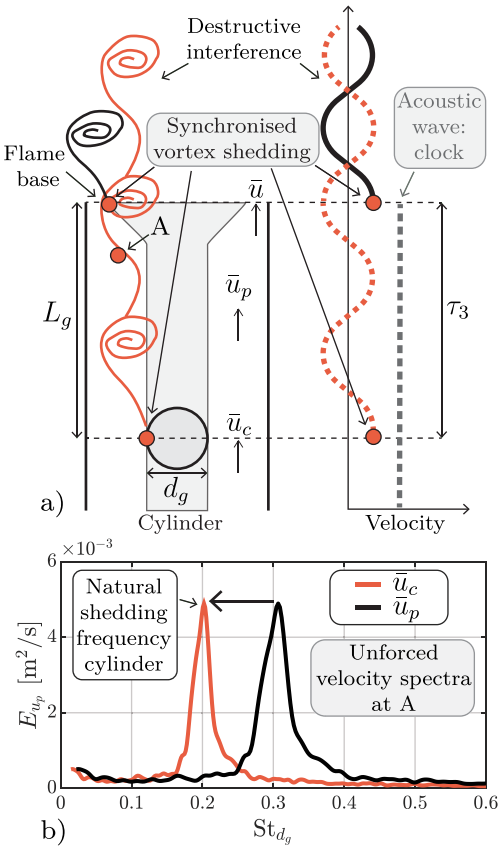

Fig. 2. (a) Schematic illustrating the acoustic/convective interference utilised to control the flame response. (b) Measurement of the unforced velocity spectra taken at location A, $3d_g$ downstream of the cylinder.

ference reduces the fluctuations in the HRR as described in detail in [31].

Briefly, the method is based on a superposition of convective disturbances associated with vortex shedding from the cylinders relative to vortex shedding at the dump plane with a relative time-delay denoted τ_3 in Figs. 1(b) and 2(a) where $\tau_3 = \tau_2 - \tau_1$. A simple explanation of the interference mechanism is illustrated in Fig. 2(a). Given the Mach number $M \ll 1$, acoustic perturbations occur approximately simultaneously at the cylinders and at the flame base which sets τ_3. When the instability frequency is sufficiently close to the natural vortex shedding frequency of the cylinders, synchronised convective waves are generated at the dump plane and the cylinder locations where the acoustic oscillations act as a clock. The flame response to these waves share the time-delay τ_1 relative to the centre of heat release rate at H (see Fig. 1b). By tuning τ_3 the degree of convective interference can be controlled by changing the cylinder position L_g as shown in Fig. 2(a) which takes advantage of the phenomenon of lock-on between the acoustic field and the vortex shedding mode of the cylinders [29]. To significantly modify the response, the procedure consists of three steps described below:

(1) *The diameter of the cylinders should be chosen such that their natural vortex shedding frequency f_n coincides with the natural frequency of the unstable mode.*

To match frequencies around 400 Hz, the cylinder diameter d_g and the bulk velocity in the inlet pipe $\bar{u}_p$ were scaled based on the optimal Strouhal number.

$$\mathrm{St}_{d_g} = \frac{f_n d_g}{\bar{u}_p} \approx 0.3. \tag{1}$$

Three cylinders with diameter $d_g = 5$ mm (see Fig. 1(b)) were chosen for a constant bulk velocity of $\bar{u} = 10$ m/s at the dump plane. As shown in Fig. 2(a), the characteristic velocity in the pipe is $u_p = 5.7$ m/s and gives us $\mathrm{St}_{d_g} \approx 0.3$. However, if we define the velocity scale at the mid-plane of the cylinders $\bar{u}_c = 8.6$ m/s due to the change in flow area around the cylinders we obtain a $\mathrm{St}_{d_g} \approx 0.2$. A measurement of the unforced velocity energy spectra is shown in Fig. 2(b) which shows how the choice of velocity scale affects the normalised natural vortex shedding frequency. Interestingly, when choosing Strouhal number based on $\bar{u}_c$ ($\mathrm{St}_{d_g} \approx 0.2$, shown by the red line), we recover the classical scaling of the Kármán vortex street [32]. However, the correct velocity scale for the Strouhal number is the velocity of the approach flow ($\bar{u}_p$) and deviations to classical scaling are expected given this is an internal flow.

(2) *The cylinders should be placed sufficiently close to the flame such that the convective fluctuations are of similar order to the acoustic fluctuations.*

Measurements were taken with the 5 mm cylinders for a range of locations $L_g/d_g < 7$ ($L_g <$ 35 mm). These are the "control-cases" shown in the second row of Tab. 1. To quantify the system response without the influence of the cylinders, a set of smaller cylinders (2 mm) were placed sufficiently far upstream ($L_g/d_g > 30$) to ensure that the vortices have decayed. These were required to center the bluff body in the injector pipe. The cases are referred to as the "no-cylinder" cases shown in the first row of Tab. 1 as the wake is mixed out by the injector exit.

(3) The minimum gain is obtained by matching the time-delay normalised by the oscillation frequency $f\tau_3 = 0.5$, 1.5, and 2.5, where $\tau_3 = L_g/\bar{u}_p$ as shown in Figs. 1(b) and 2(a).

For cylinders in a cross flow, these values are predictable due to the simple nature of the convective wave propagation inside the pipe [28,31]

The stability of the system was measured while varying the equivalence ratio Φ and cylinder location L_g systematically. A total of 42 conditions were tested. The range $L_g/d_g = [4 - 7]$ corresponding to $f\tau_3 = [1.4 - 2.45]$ was chosen. This corresponds to

Please cite this article as: E. Æsøy, G.K. Jankee, S. Yadala et al., Suppression of self-excited thermoacoustic instabilities by convective-acoustic interference, Proceedings of the Combustion Institute, https://doi.org/10.1016/j.proci.2022.08.033

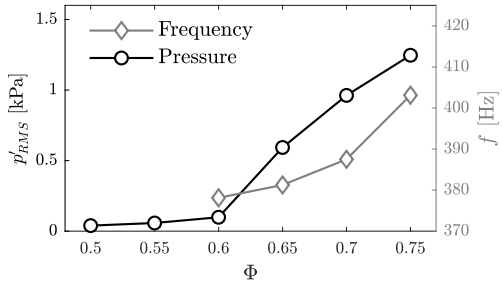

Fig. 3. (a) Stability map for the "no-cylinder" cases: RMS fluctuations of pressure (p'_1) and oscillation frequency plotted against equivalence ratio.

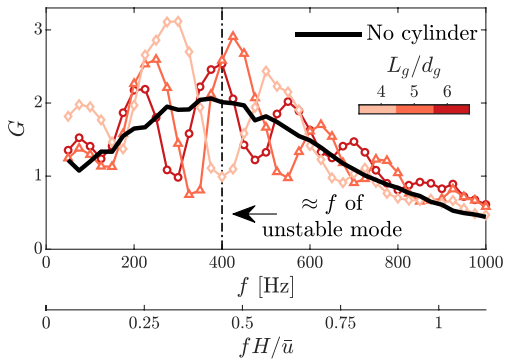

Fig. 4. Gain of the FTF at $\Phi = 0.7$.The cylinders modifies the gain by introducing modulations.

a range of $f\tau_3$ where the interference is predicted to change from being destructive close to $L_g/d_g = 4$ and 7, and constructive close to 6.

2.4. FTF measurements

For completeness and to supplement discussion of the results, FTFs were also measured to relate changes in the self-excited system stability to the forced flame response. Using the 5 mm cylinders, FTFs were measured for $\Phi = 0.7$ at 7 locations in the range $L_g/d_g = [4 - 7]$ and for the no cylinder case. When measuring FTFs the shorter quartz combustion chamber ($L_c = 80$ mm) was used to ensure stable operating conditions with the same flame shape. Acoustic forcing was provided by two Monacor KU-516 horn drivers mounted in the plenum section and driven by a QTX Sound PRO1000 power amplifier. The forcing signal p_{ref} was generated using an Aim-TTi TGA1244 signal generator to generate harmonic velocity oscillations with a constant amplitude of $|\hat{u}|/\bar{u} = 0.05$ over the measured frequency range of $50 - 1000$ Hz, following the same procedure as in [11,31].

The FTF is defined as

$$\text{FTF}(\omega) = \frac{\hat{Q}/\bar{Q}}{\hat{u}/\bar{u}} = G\exp(j\Theta), \tag{2}$$

where $\omega = 2\pi f$ and relates the normalised fluctuations of HRR and acoustic velocity at the dump plane ($x = 0$), obtained using the multiple microphone method [38,39]. If the gain, G, is large the oscillations in HRR are amplified by the acoustic oscillations.

3. Results

3.1. Self-excited response without cylinders

First, the stability of the system is characterised for the no-cylinder cases. Fig. 3 plots how the root mean square (RMS) fluctuations of pressure, p'_{RMS}, varies with equivalence ratio, Φ. The stability map shows that the system is stable when $\Phi < 0.6$ whereas strong self-excited instabilities are produced when $\Phi \geq 0.6$. The self-excited modes correspond to the quarter wave mode of the combustion chamber. The amplitude grows quickly with increasing Φ from $0.5kPa$ at $\Phi = 0.65$ to > 1 kPa at $\Phi = 0.7$. The corresponding frequency of the self-excited mode is also shown and is found to increase with Φ due to the increase in flame temperature T_a. From $\Phi = 0.6$ to 0.75, the frequency increases by about 10% which is approximately similar to the increase in $\sqrt{T_a}$.

3.2. Tailoring the flame response

To demonstrate the effect of varying the cylinder location on the flame response, a total of eight FTFs were measured at $\Phi = 0.7$.

Fig. 4 shows the gain G of the FTF for the no cylinder case (black line) and at three cylinder positions $L_g/d_g = [4, 5, 6]$ (coloured lines). For reference, a dashed vertical line is added at $f = 400$ Hz which corresponds to the frequency of the unstable mode without cylinders present (see Fig. 3). The gain for the no cylinder case resembles a low-pass filter with peak values in the low frequency range and reduces at higher frequencies. The gain response for the different cylinder locations $L_g/d_g = [4, 5, 6]$ shows that when placed sufficiently close to the burner exit they exert a strong influence on the flame response, resulting in large amplitude modulations that significantly increase and decrease the gain. These measurements validate step (2) in Section 2.3, i.e. the cylinders are placed sufficiently close to the dump plane to have a strong impact. The modulations are superimposed on the no-cylinder case illustrating that the response is due to convective-acoustic interference [28].

When L_g is varied, the frequencies where gain maxima and minima occur shift due to a change of the convective-acoustic time-delay τ_3. Since $\bar{u}_p$

Please cite this article as: E. Æsøy, G.K. Jankee, S. Yadala et al., Suppression of self-excited thermoacoustic instabilities by convective-acoustic interference, Proceedings of the Combustion Institute, https://doi.org/10.1016/j.proci.2022.08.033

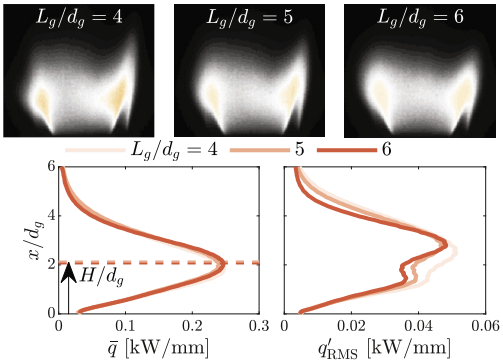

Fig. 5. Mean flame OH* images and stream-wise integrated profiles of the mean an RMS fluctuations in the HRR for varying cylinder position.

is kept constant, the frequency shift of the modulations is proportional to L_g. When $L_g/d_g = 4$, the time-delay is shorter than at $L_g/d_g = 6$ and hence, the maxima and minima of the FTF appear at higher frequencies.

The effect of the cylinders can also be seen in Fig. 5 where the mean flame shapes are shown for $L_g/d_g = [4, 5, 6]$. The integrated profiles of the mean and RMS HRR, $\bar{q}$ and q'_{RMS}, are shown below. Although the flame shape is slightly modified when the image plane lies across one cylinder (see Fig. 1(b)), the flame length which determines the mean time-delay τ_1 and cut-off frequency [11,12], remains similar. This is confirmed by the collapse of the FTFs for the different L_g at higher frequencies as shown in Fig. 4. The effect of the cut-off frequency is also illustrated with the additional axis in Fig. 4, where the gain G drops exponentially for $fH/\bar{u} > 1$. Here, H is defined as the barycenter of the mean HRR $\bar{q}$ ($H = \int x\bar{q}\mathrm{d}x / \int \bar{q}\mathrm{d}x$) integrated in the transverse direction direction. There is, however, a small increase in the RMS fluctuations due to the presence of the cylinders.

Following the same analysis as in [31], parameters are extracted from the FTFs by fitting them to a distributed time lag (DTL) model:

$$\mathrm{DTL_T}(\omega) = \mathrm{DTL_1} + \mathrm{DTL_2} \tag{3}$$

$$\mathrm{DTL}_i = E_i^+ + E_i^- \tag{4}$$

$$E_i^{\pm} = \frac{g_i}{2}\exp\left(-\frac{1}{2}(\omega \pm \beta_i)^2\sigma_i^2 - j\omega\tau_i\right), \tag{5}$$

where g_i, ω_i, β_i, and τ_i are model constants. The model is only used here to demonstrate consistency between the model parameters and the physics underpinning the three-step procedure.

The model represents the flame response as a superposition of two delayed responses with distributions $\mathrm{DTL_1}$ and $\mathrm{DTL_2}$ in the frequency domain. The modulation frequency β_i corresponds to the preferred frequency where the maximum response of each distribution occurs and g_i, σ_i^2, and τ_i are the gain, variance, and mean time-delay respectively. In the time domain these correspond to impulse response functions [40]. For more details of the procedure and description of the model see [11].

In Fig. 6(a,b) the important parameters τ_3 and β_2 are respectively plotted against $L_g/\bar{u}_p$ and L_g/d_g. The extracted time-delay τ_3 is equal to $L_g/\bar{u}_p$, as was also shown in [11,31]. The modulation frequency is approximately a constant $\beta_2 \approx 350$ Hz, corresponding to $\mathrm{St}_{d_g} \approx 0.3$, consistent with the vortex shedding frequency. This is expected as moving the cylinder does not change its natural vortex shedding frequency and hence $\beta_2 \approx f_n$.

Using the DTL model, the gain and phase modulations can be expressed by:

$$\frac{\Delta G}{G} = \left|\frac{\mathrm{FTF}}{\mathrm{DTL_1}}\right| - 1, \quad \Delta\Theta = \angle\frac{\mathrm{FTF}}{\mathrm{DTL_1}}. \tag{6}$$

If $\Delta G/G > 0$, the gain of the FTF is increased and if $\Delta G/G < 0$ the gain is reduced. Similarly, $\Delta\Theta$ quantifies the changes to the phase/time-delay.

Model parameters are extracted for all cases and the modulations are shown in Fig. 6(c–e). In Fig. 6(c) the gain modulations are plotted against Strouhal number based on the cylinder diameter St_{d_g} defined in Eq. (1). The dimensional frequency is also shown for ease of interpretation. As predicted, the modulations are approximately centred at the cylinder's natural shedding frequency at $\mathrm{St}_{d_g} \approx 0.3$ (see Fig. 2(b)). Changing L_g does not change the shedding frequency but instead shifts the modulations within the envelope defined by $|\mathrm{DTL_2}|/|\mathrm{DTL_1}|$ indicated by the black lines. As discussed in [31], the envelope quantifies the frequency range where lock-in with vortex-shedding from the cylinder occurs.

To show that τ_3 determines the frequency shift of the modulations, the modulations are plotted against the normalised frequency $f\tau_3$ in Fig. 6(d,e). When scaled by τ_3, the modulations collapse on top of each other and the wavelength of the modulations is unity. At $f\tau_3 = 1$ and 2, the interference is constructive, increasing the gain to peak values. Conversely, at $f\tau_3 = 0.5$, 1.5. and 2.5, the interference is destructive reducing the gain to minimum values. Fig. 6(e) shows that at $f\tau_3 = 0.75$, 1.25, 1.75, and 2.25, significant changes to the phase Θ are present, altering the time-delay. The black lines in (d) and (e) correspond to $\cos(2\pi f\tau_3)$ and $\sin(2\pi f\tau_3)$, which are proportional to $\Delta G/G$ and $\Delta\Theta$ respectively.

We emphasise that the results presented in this section demonstrate that the scaling of ΔG and $\Delta\Theta$ with L_g and $\bar{u}_p$ are simple to predict and hence, measurements of the FTF are not needed to implement the method which is demonstrated next.

Please cite this article as: E. Æsøy, G.K. Jankee, S. Yadala et al., Suppression of self-excited thermoacoustic instabilities by convective-acoustic interference, Proceedings of the Combustion Institute, https://doi.org/10.1016/j.proci.2022.08.033

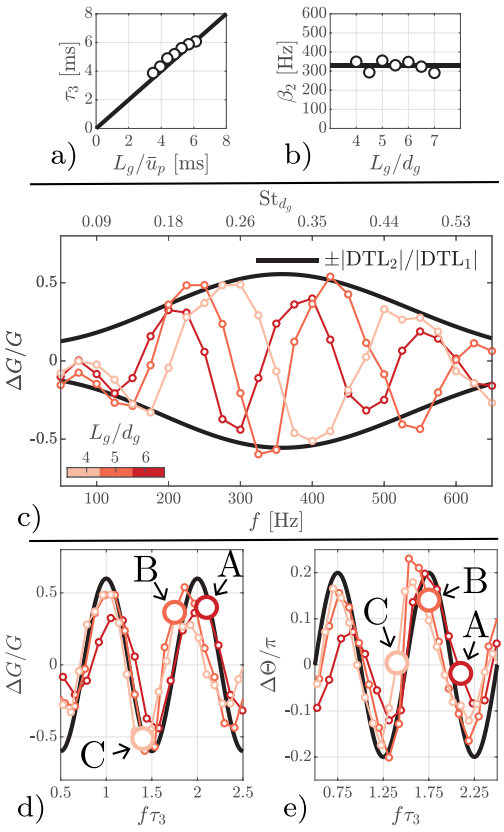

Fig. 6. (a,b) variation of DTL parameters $\tau_3 = \tau_2 - \tau_1$ and β_2 with L_g. (c and d) Gain ($\Delta G/G$) and e) phase ($\Delta\Theta/\pi$) modulations. d) and e) are plotted against the normalised frequency $f\tau_3$ aligning the modulations. The black lines in d) and e) correspond to $\cos(2\pi f\tau_3)$ and $\sin(2\pi f\tau_3)$, which are proportional to $\Delta G/G$ and $\Delta\Theta$, respectively. A, B, and C correspond to $f = 400$ Hz for $L_g/d_g = 6$, 5, and 4, respectively.

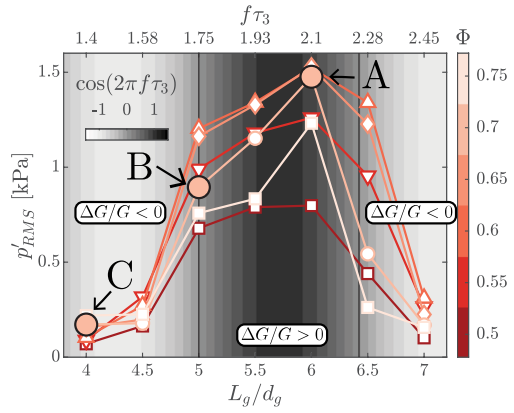

Fig. 7. Stability map for the "control-cases": RMS fluctuations of pressure (p'_1) with the cylinders placed at different positions L_g/d_g. The background colour correspond to $\cos(2\pi f\tau_3)$, which is proportional to $\Delta G/G$ (see Fig. 6(d)).

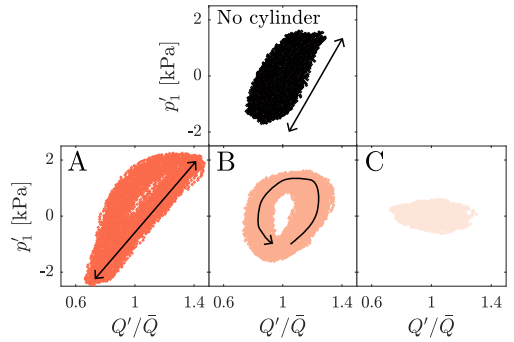

Fig. 8. Phase-portraits at $\Phi = 0.7$ plotting p'_1 against Q' for the "no cylinder" case and with cylinders placed at A, B, and C, corresponding respectively to $L_g/d_g = [6, 5, 4]$ and $f\tau_3 = [2.1, 1.75, 1.4]$.

3.3. Controlling the self-excited response

The next step is to measure the amplitude of the self-excited instabilities for varying cylinder position, L_g. Fig. 6 shows that to minimise the gain, L_g should be chosen to give $f\tau_3 = 0.5$, 1.5, or 2.5 at the self-excited frequency $f \approx 400$ Hz (see Fig. 3).

The response of the self-excited modes to varying L_g is shown in Fig. 7 which plots the RMS of the pressure fluctuations, p'_{RMS}, against L_g. The different colors correspond to different equivalence ratios shown in the range $\Phi = [0.5, 0.75]$ which is the same range as in Fig. 3. The background colour shows the gain response predicted by the $f\tau_3$ scaling which takes the form $\cos(2\pi f\tau_3)$ and is proportional to $\Delta G/G$, similar to the black line in Fig. 6(d).

Fig. 7 shows that varying L_g leads to significant changes in the amplitude of the pressure oscillations. The system is unstable for all values of Φ in the region $5 < L_g/d_g < 6.5$ and stable for $L_g/d_g < 5$ and $L_g/d_g > 6.5$. These regions closely coincide to the regions where the gain of the FTF is increased and decreased and is directly correlated to the normalised convective-acoustic time-delay $f\tau_3$. As predicted, maximum damping of the instability amplitude occurs when $f\tau_3 = 1.5$ and 2.5, whereas maximum amplitude occurs when $f\tau_3 = 2$. Furthermore, these values of $f\tau_3$ are independent of Φ. This has important implications since changes to the flame properties on the thermoacoustic behaviour are harder to predict. Hence, this method is potentially well suited for fuel flexible systems.

To illustrate the influence of different cylinder positions on the flame dynamics, phase portraits of Q' and p'_1 are plotted in Fig. 8. The cylinder positions $L_g/d_g = [6, 5, 4]$ are annotated as A, B, and C. These correspond to $f\tau_3 \approx [2, 1.75, 1.5]$, where re-

Please cite this article as: E. Æsøy, G.K. Jankee, S. Yadala et al., Suppression of self-excited thermoacoustic instabilities by convective-acoustic interference, Proceedings of the Combustion Institute, https://doi.org/10.1016/j.proci.2022.08.033

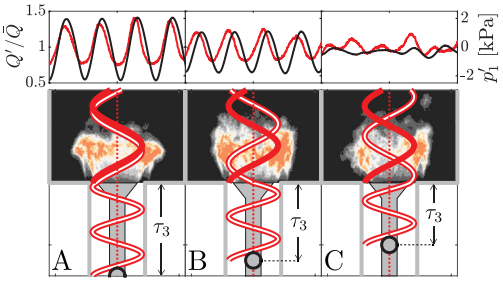

Fig. 9. Time series of p_1' (black) and Q' (red) and snapshots of the convective waves with cylinders placed at A, B, and C, corresponding respectively to $L_g/d_g = [6, 5, 4]$ and $f\tau_3 = [2.1, 1.75, 1.4]$.

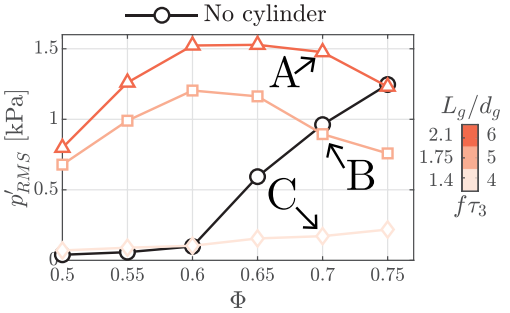

Fig. 10. Stability map comparing the "no cylinder" case with the "control-cases", where the cylinders are placed at $L_g/d_g = [6, 5, 4]$, correspond respective to $f\tau_3 = [2.1, 1.75, 1.4]$. Matching $f\tau_3 \approx 1.5$ stabilises the system for all values of Φ.

spectively $\Delta G/G > 0$, $\Delta\Theta > 0$ and $\Delta G/G < 0$ (see Fig. 6). The top panel shows the case without the influence of the cylinders.

In panel A, where $\Delta G/G > 0$, the amplitudes of Q' and p_1' are greater than the no-cylinder case. However, the shapes of the phase portraits are somewhat similar, showing that the phase is not significantly altered. This is consistent with Fig. 6(e) where $\Delta\Theta \approx 0$. The trajectory formed resembles an approximately straight line with a positive slope and indicates that Q' and p_1' are oscillating in phase where the maximum and minimum values coincide.

In panel B a circular pattern in the phase portrait emerges. However, the amplitudes of Q' and p_1' are similar to the no-cyclinder case. The different response is due to the shift of the phase $\Delta\Theta$ which is large at $f\tau_3 \approx 1.75$ (see Fig. 6(e)). Due to the phase shift, the trajectory resembles an orbital pattern indicating that Q' and p_1' now lag each other. Considering the Rayleigh criterion, a change in the phase should also alter the amplitude of the limit-cycle. In this case it should reduce due to the de-phasing of Q' and p_1'. Although at $f\tau_3 = 1.75$, the gain modulations should be small, Fig. 6(d) shows that $\Delta G/G > 0$, which compensates for the change in the phase. This feature is also observed in the phase portrait where the amplitude of Q' in B is larger compared to the no-cylinder case. This suggests that the strategy of tuning the phase by matching $f\tau_3 = [1.25, 1.75, 2.25]$ may be less robust than tuning the gain.

In panel C where $f\tau_3 \approx 1.5$ is matched, the pressure fluctuations are significantly reduced and the system is stabilised. The reduction in the pressure amplitude results from destructive interference cancelling the coherent part of Q'.

To illustrate how the two convective waves interact, time series of p_1' and Q' along with a sketch of the convective waves inside the injector pipe and along the flame are shown in Fig. 9. At A, the two waves are in phase driving oscillations, at B, they are a quarter period out of phase leading to a delay between p' and Q', and at C they are out of phase leading to stable operation.

The cases in Figs. 8 and 9 are only shown for $\Phi = 0.7$. To demonstrate that the method works over the full range of Φ, a stability map for the cylinder positions $L_g/d_g = [6, 5, 4]$ as well as the no-cylinder case are shown in Fig. 10. The annotations A, B, and C correspond to the phase portraits in Fig. 8. As discussed above, at A the amplitude of p_1' is increased, at B p_1' is similar, and at C p_1' is significantly reduced.

By matching $f\tau_3 \approx 1.5$, p_1' is reduced for all values of Φ. This shows that the method can control the onset of thermoacoustic instabilities for a fuel flexible system where the goal is to operate in a wide range of operating conditions. However, caution must be exercised as the cyclinders can also be used to destabilse the system. This is illustrated when $\Phi < 0.65$ for the case when the cylinders are located at $L_g/d_g = 5$ and 6. In these cases the gain is increased compared to the no-cylinder case. The method presented herein relies on a predictable scaling of the time-delay τ_3 which is straight forward for cylinders in a uniform flow where the shedding frequency is well understood. Determining τ_3 is not trivial for more complex geometries and flows, for example with swirlers which have a significant azimuthal velocity component [19,20,23,31,33].

4. Conclusion

In this paper we demonstrate that self-excited thermoacoustic instabilities can be controlled using targeted convective-acoustic interference. The method recently proposed in [31] is implemented and tested on a laboratory scale combustor. Cylinders are placed upstream of the flame to generate targeted interference between synchronised vortex shedding from the cylinders and the acous-

Please cite this article as: E. Æsøy, G.K. Jankee, S. Yadala et al., Suppression of self-excited thermoacoustic instabilities by convective-acoustic interference, Proceedings of the Combustion Institute, https://doi.org/10.1016/j.proci.2022.08.033

tic forcing driving HRR oscillations. Tuning of the time-delay between the vortex shedding from the cylinders and the flame is achieved by varying the position of the cylinders to promote destructive convective-acoustic interference and damp the flame response suppressing the self-excited mode. The method is based on careful tuning of a hydrodynamic instability and hence is not dependent on the flame parameters. Measurements were taken with and without cylinders for a wide range of equivalence ratios to demonstrate that the method is capable of stabilising the system for a wide range of operating conditions, demonstrating its potential application to fuel flexible combustion systems.

Declaration of Competing Interest

The authors declare that they have no known competing financial interests or personal relationships that could have appeared to influence the work reported in this paper.

Acknowledgments

The authors would like to acknowledge financial support from the Norwegian Research Council, Project No.: 257579/E20 (FME Norwegian CCS Research Centre) and 299946, and the European Research Council (ERC): Grant agreement 677931 TAIAC.

References

[1] G.A. Richards, M.M. McMillian, R.S. Gemmen, W.A. Rogers, S.R. Cully, Issues for low-emission, fuel-flexible power systems, PECS 27 (2001) 141–169.
[2] S. Candel, Combustion dynamics and control: progress and challenges, Proc Combust Inst. 29 (2002) 1–28.
[3] T.C. Lieuwen, V. Yang, Combustion instabilities in gas turbine engines: operational experience, fundamental mechanisms, and modeling, 3, AIAA, 2005.
[4] M.R. Bothien, A. Ciani, J.P. Wood, G. Fruechtel, Sequential combustion in gas turbines: the key technology for burning high hydrogen contents with low emissions, 4A, ASME, 2019.
[5] ETN, Hydrogen gas turbines: The path towards a zero-carbon gas turbine, 2020,.Tech. rep., ETN Global.
[6] K.C. Schadow, E. Gutmark, Combustion instability related to vortex shedding in dump combustors and their passive control, PECS 18 (1992) 117–132.
[7] T.C. Lieuwen, Unsteady Combustor Physics, CUP, 2021.
[8] L. Rayleigh, The explanation of certain acoustical phenomena, R. Inst. Proc. 8 (1878) 536–542.
[9] K.T. Kim, J.G. Lee, B.D. Quay, D.A. Santavicca, Response of partially premixed flames to acoustic velocity and equivalence ratio perturbations, Combust. Flame 9 (2010) 1731–1744.
[10] T. Schuller, D. Durox, S. Candel, A unified model for the prediction of laminar flame transfer functions: comparisons between conical and v-flame dynamics, Combust. Flame 1 (2003) 21–34.
[11] E. Æsøy, J.G. Aguilar, S. Wiseman, M.R. Bothien, N.A. Worth, J.R. Dawson, Scaling and prediction of transfer functions in lean premixed H2/CH4-flames, Combust. Flame 215 (2020) 269–282.
[12] E. Æsøy, T. Indlekofer, F. Gant, A. Cuquel, M.R. Bothien, J.R. Dawson, The effect of hydrogen enrichment, flame-flame interaction, confinement, and asymmetry on the acoustic response of a model can combustor, Combust. Flame 242 (2022) 112176.
[13] N. Noiray, D. Durox, T. Schuller, S. Candel, A unified framework for nonlinear combustion instability analysis based on the flame describing function, J. Fluid Mech. 615 (2008) 139–167.
[14] T. Schuller, T. Poinsot, S. Candel, Dynamics and control of premixed combustion systems based on flame transfer and describing functions, J. Fluid Mech. 894 (2020).
[15] D.L. Straub, G.A. Richards, Effect of axial swirl vane location on combustion dynamics, 78590, ASME, 1999.
[16] K. McManus, T. Poinsot, S. Candel, A review of active control of combustion instabilities, PECS 19 (1993) 1–29.
[17] P. Berenbrink, S. Hoffmann, Suppression of dynamic combustion instabilities by passive and active means, 78552, ASME, 2000.
[18] N. Noiray, D. Durox, T. Schuller, S. Candel, Dynamic phase converter for passive control of combustion instabilities, Proc Combust Inst. 32 (2009) 3163–3170.
[19] T. Komarek, W. Polifke, Impact of swirl fluctuations on the flame response of a perfectly premixed swirl burner, J. Eng. Gas Turbines Power 132 (2010).
[20] P. Palies, D. Durox, T. Schuller, S. Candel, The combined dynamics of swirler and turbulent premixed swirling flames, Combust. Flame 157 (2010) 1698–1717.
[21] K.T. Kim, D.A. Santavicca, Interference mechanisms of acoustic/convective disturbances in a swirl-stabilized lean-premixed combustor, Combust. Flame 160 (2013) 1441–1457.
[22] M. Gatti, R. Gaudron, C. Mirat, L. Zimmer, T. Schuller, A comparison of the transfer functions and flow fields of flames with increasing swirl number, 4b, ASME, 2018.
[23] H.T. Nygård, N.A. Worth, Flame transfer functions and dynamics of a closely confined premixed body stabilised flame with swirl, J. Eng. Gas Turbines Power 143 (2021).
[24] P. Palies, D. Durox, T. Schuller, S. Candel, Experimental study on the effect of swirler geometry and swirl number on flame describing functions, Combust. Sci. Technol. 183 (2011) 704–717.
[25] P. Palies, D. Durox, T. Schuller, S. Candel, Acoustic convective mode conversion in an aerofoil cascade, J. Fluid Mech. 672 (2011) 545–569.
[26] W. Polifke, Black-box system identification for reduced order model construction, Ann. Nucl. Energy 67 (2014) 109–128.
[27] A. Huber, W. Polifke, Dynamics of practical premixed flames, part II: identification and interpretation of CFD data, Int. J. Spray Combust. Dyn. 1 (2009) 229–249.

[28] E. Æsøy, J.G. Aguilar, M.R. Bothien, N.A. Worth, J.R. Dawson, Acoustic-convective interference in transfer functions of methane/hydrogen and pure hydrogen flames, J. Eng. Gas Turbines Power 143 (2021).
[29] R. Blevins, The effect of sound on vortex shedding from cylinders, J. Fluid Mech. 161 (1985) 217–237.
[30] B. Herrmann, P. Oswald, R. Semaan, S.L. Brunton, Modeling synchronization in forced turbulent oscillator flows, Commun. Phys. 3 (2020) 1–9.
[31] E. Æsøy, H.T. Nygård, N.A. Worth, J.R. Dawson, Tailoring the gain and phase of the flame transfer function through targeted convective-acoustic interference, Combust. Flame 236 (2022) 111813.
[32] A. Roshko, On the development of turbulent wakes from vortex streets, No NACA-TR-1191 (1953).
[33] A. Albayrak, M.P. Juniper, W. Polifke, Propagation speed of inertial waves in cylindrical swirling flows, J. Fluid Mech. 879 (2019) 85–120.
[34] D. Durox, J.P. Moeck, J. Bourgouin, P. Morenton, M. Viallon, T. Schuller, S. Candel, Flame dynamics of a variable swirl number system and instability control, Combust. Flame 160 (2013) 1729–1742.
[35] D.M. Reuter, Investigation of Combustion Instability in Ramjet Combustors, Georgia Inst. of Tech., Atlanta, GA (USA), 1988. Technical Report
[36] U. Hegde, D. Reuter, B. Zinn, Combustion instability mechanisms in ramjets, in: Proceedings of the 26th Aerospace Sciences Meeting, 1988, p. 150.
[37] B. Higgins, M.Q. McQuay, F. Lacas, J.C. Rolon, N. Darabiha, S. Candel, Systematic measurements of OH chemiluminescence for fuel-lean, high-pressure, premixed, laminar flames, Fuel 80 (2001) 67–74.
[38] A.F. Seybert, D.F. Ross, Experimental determination of acoustic properties using a two microphone random excitation technique, J. Acoust. Soc. 61 (1977) 1362–1370.
[39] E. Æsøy, The Effect of Hydrogen Enrichment on the Thermoacoustic Behaviour of Lean Premixed Flames, PhD thesis, NTNU, 2022.
[40] W. Polifke, Modeling and analysis of premixed flame dynamics by means of distributed time delays, PECS 79 (2020) 100845.

Please cite this article as: E. Æsøy, G.K. Jankee, S. Yadala et al., Suppression of self-excited thermoacoustic instabilities by convective-acoustic interference, Proceedings of the Combustion Institute, https://doi.org/10.1016/j.proci.2022.08.033